ACS OMEGA

Open Access

http://pubs.acs.org/journal/acsodf

Article

Redox-Active Phenanthrenequinone Molecules and Nitrogen-Doped Reduced Graphene Oxide as Active Material Composites for Supercapacitor Applications

Navid Noor, Thomas Baker, Hyejin Lee, Elliot Evans, Shayan Angizi, Jeffrey Daniel Henderson, Amirhossein Rakhsha, and Drew Higgins*

Cite This: *ACS Omega* 2024, 9, 10080−10089

Read Online

ACCESS | Metrics & More | Article Recommendations | Supporting Information

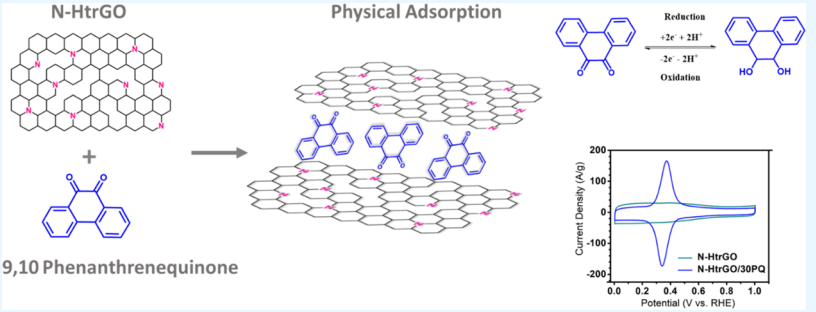

ABSTRACT: Carbon-based supercapacitor electrodes are generally restricted in energy density, as they rely exclusively on electric double-layer capacitance (EDLC). The introduction of redox-active organic molecules to obtain pseudocapacitance is a promising route to develop electrode materials with improved energy densities. In this work, we develop a porous nitrogen-doped reduced graphene oxide and 9,10-phenanthrenequinone composite (N-HtrGO/PQ) via a facile one-step physical adsorption method. The electrochemical evaluation of N-HtrGO/PQ using cyclic voltammetry showed a high capacitance of 605 F g^{-1} in 1 M H_2SO_4 when the composite consisted of 30% 9,10-phenanthrenequinone and 70% N-HtrGO. The measured capacitance significantly exceeded pure N-HtrGO without the addition of redox-active molecules (257 F g^{-1}). In addition to promising capacitance, the N-HtrGO/30PQ composite showed a capacitance retention of 94.9% following 20,000 charge/discharge cycles. Based on Fourier transform infrared spectroscopy, we postulate that the strong $\pi-\pi$ interaction between PQ molecules and the N-HtrGO substrate enhances the specific capacitance of the composite by shortening pathways for electron transfer while improving structural stability.

1. INTRODUCTION

The consequence of climate change caused by greenhouse gas emissions from fossil fuel consumption has led to an urgent global demand for green and sustainable energy technologies. Energy storage devices are becoming an increasingly sought-after technology to address energy sustainability challenges. Supercapacitors, also called electrochemical capacitors, are energy storage devices that can provide high power density, a long life span, and rapid charging/discharging.[1−4] These properties render them attractive for various applications, including electric vehicles, portable electric devices, and emergency backup power systems. Unfortunately, the low energy density of supercapacitors is one factor hindering their practical application.[5]

Supercapacitors employ two main mechanisms by which they store charge: electrical double-layer capacitance (EDCL) and pseudocapacitance. In EDLC, ions are absorbed on the electrode/electrolyte interface during charge and desorbed during discharge.[1,5,6] Electrode materials having high specific surface area and electrical conductivity are utilized in supercapacitors relying on electrical double-layer capacitance. Among different groups of materials employed, carbon materials, including graphene, carbon nanotubes, and carbon blacks, have shown promising performance of EDLC due to their high surface areas, good electrical conductivity, chemical stability, and low production cost.[1,6,7] Graphene is a two-dimensional carbon-based material that benefits from possessing the highest theoretical surface area among graphitic carbons as, in principle, they are two-dimensional monolayer sheets.[8−11] Furthermore, starting with graphene oxide (GO) as a precursor, it is possible to functionalize graphene in different ways, which is nontrivial when starting with relatively inert

Received: July 6, 2023
Revised: January 24, 2024
Accepted: February 5, 2024
Published: February 22, 2024

graphitic carbon precursors. These characteristics render graphene a promising material candidate for improving electrical double-layer capacitance.[12−16] Despite attractive properties, two-dimensional monolayer graphene sheet restacking is a severe issue that needs to be addressed. Sheet restacking leads to a decrease in specific surface area and, by extension, electrochemical double-layer capacitance. Heteroatoms such as nitrogen and sulfur incorporated into the structure of graphene layers can act as molecular spacers to reduce stacking and improve hydrophilicity, which enhances electrolyte permeation into the electrode structures. Nitrogen-doped reduced graphene oxide (N-HtrGO) has high electrical conductivity and does not suffer from restacking, which makes it a favorable candidate for supercapacitor applications.[17−20] In our previous work,[6] we investigated the impact of nitrogen doping and amine functionalization of reduced graphene oxide on the capacitance of the materials. Three different nitrogen-containing compounds: nitrogen-doping (N-HtrGO), amine-functionalization (NH_3^+-HtrGO), and hybrid amine-functionalization and nitrogen-doping (N-NH_3^+-HtrGO), were synthesized. The highest specific capacitance of 244 F g^{-1} was achieved by N-HtrGO, measured by using cyclic voltammetry at a scan rate of 50 mV s^{-1} in 1 M sulfuric acid. The lowest specific capacitance was 179 F g^{-1} at 50 mV s^{-1} for NH_3^+-HtrGO. The specific capacitance of N-NH_3^+-HtrGO was between N-HtrGO and NH_3^+-HtrGO. Even with functionalization and doping, the achieved capacitance was still lower than previous reports,[21−23] and further improvements to the power density and energy density of these electrical double-layer capacitor materials are still needed.

One route to improve supercapacitor performance beyond that of an EDLC active material is by incorporating a second charge storage mechanism, pseudocapacitance, which can increase the total capacitance and energy density. Pseudocapacitive materials store charge by redox (Faradaic) reactions in the presence of an electrolyte.[24] Similar to electrical double-layer capacitance, pseudocapacitance is also an ultrafast mechanism.[25−27] Various materials, including transition metal oxides, MXenes, conductive polymers, and redox organic molecules, have been widely studied as pseudocapacitive electrode materials.[28−34] Particularly, quinones and their derivatives can be employed for supercapacitor applications owing to their intrinsic electrochemical redox activity.[35−38] These organic molecules have controllable structures that can be tuned by modifying the number of aromatic groups and changing the identity and location of their attached functional groups.[39,40] The organic backbones of these molecules are stable when undergoing Faradaic reactions, experiencing minimal structural changes, unlike metal oxides. Furthermore, Wedege et al.[41] showed that using quinones for application in energy storage devices is economically feasible. However, quinone compounds possess poor intrinsic electrical conductivity and are prone to poor cycling stability due to dissolution in aqueous electrolytes, which hampers their practical suitability.[42] To overcome conductivity limitations and mitigate dissolution into the electrolyte, organic molecules can be anchored on the surface of conductive carbon scaffolds.[43,44] Covalent and noncovalent modifications are two approaches undertaken to bind organic molecules to carbon substrates, including reduced graphene oxide.[45] Covalent modification can be done via chemical reactions, which might affect the carbon atom hybridizations in the substrate and transform sp^2-bonded carbon into sp^3-bonded carbon, detrimentally impacting the electrical conductivity.[45,46] Conversely, noncovalent modification is based on a physical process, for example, $\pi-\pi$ interactions.[47] Therefore, the formation of a $\pi-\pi$ network between organic redox-active molecules and graphene and its derivatives would not affect the structure of graphene and its properties. In addition, noncovalent bonding through a physical adsorption process is more cost-effective than the use of energy-intensive synthesis processes like hydrothermal and solvothermal. Several studies have been performed on modifying graphene-based material with quinones and quinone derivatives, whereby quinone molecules can act as a molecular spacer to weaken $\pi-\pi$ interactions between graphene layers and decrease restacking.[35] In one study, Guo et al.[39] used three different anthraquinones, including anthraquinone (AQ), 1,4-naphthoquinone (NQ), and tetrachlorobenzoquinone (TCBQ), to modify a nitrogen-doped porous carbon derived from a metal−organic framework. The asymmetrical supercapacitor showed a specific capacitance of 86 F g^{-1} at a current density of 1 A g^{-1} and an energy density of 23.5 Wh kg^{-1} at 0.7 kW kg^{-1}. Xu et al.[48] used 1,4,5,8-tetrahydroxy anthraquinone (THAQ) to prepare redox-active electrode through physical adsorption on reduced graphene oxide (rGO). The THAQ/rGO composite showed a specific capacitance of 259 F g^{-1} at 1 A g^{-1} and a capacitance retention of 97.9% after 10,000 cycles. In another study, Xu et al.[49] used indole molecules to functionalize nitrogen-doped reduced graphene oxide. This material showed an outstanding capacitance of 622 F g^{-1} at 2 A g^{-1} and a high capacitance retention of 101% after 5000 charging/discharging cycles. Despite advances in the literature, much of the high performance observed came at the cost of complex supercapacitor material synthesis processes that may not be practical for large-scale manufacturing. The development of a simpler synthetic process is desirable to prepare supercapacitor materials with high overall capacitance and stable pseudocapacitive contributions.[6,50]

In this work, we develop composite supercapacitor electrode active materials by deploying a simple one-step physical mixing process to anchor 9,10-phenanthrenequinone (PQ) on nitrogen-doped reduced graphene oxide. 9,10-Phenanthrenequinone is a small organic molecule that consists of three aromatic rings and two carbonyl groups that provide redox activity in the presence of protons,[51] while the nitrogen-doped reduced graphene oxide provides a high surface area and electron conductivity as a substrate. Nitrogen doping has the added advantage of increasing the electrical conductivity[52] and hydrophilicity[53−55] in comparison with undoped reduced graphene oxide. Additionally, nitrogen doping of the rGO has been found to decrease graphene layer restacking.[56] Fourier transform infrared (FTIR) spectroscopy results showed the formation of a $\pi-\pi$ network between the reduced graphene oxide and 9,10-phenanthrenequinone. The composite structure showed a specific capacitance of 605 F g^{-1} measured by CV at 50 mV s^{-1} in 1 M sulfuric acid, representing a marked improvement over that of pure N-HtrGO (257 F g^{-1}). These results show that the redox-active PQ molecules provide high pseudocapacitance, which contributes to the high specific capacitance of the composite. Furthermore, a 94.9% capacitance retention was achieved after 20,000 charge/discharge cycles, which could be attributed to the existence of the $\pi-\pi$ network between the PQ molecules and N-HtrGO surface. Thus, this approach paves the way for preparing supercapacitor materials by a facile procedure to

https://doi.org/10.1021/acsomega.3c04836
ACS Omega 2024, 9, 10080−10089

composite high-surface-area EDLC materials with pseudocapacitive molecules in an electrochemically stable configuration.

2. EXPERIMENTAL METHODS

2.1. Chemicals. Graphene oxide (GO) was purchased from Graphenea Inc. (Spain) and used as received. 9,10-Phenanthrenequinone (PQ) was purchased from TCI Co. Sulfuric acid (H_2SO_4), ethanol, Nafion-117-containing solution (5 wt % in a mixture of lower aliphatic alcohols and water), and urea were obtained from Sigma-Aldrich. All solutions were prepared using Type 1 ultrapure water (>18 MΩ·cm, Millipore).

2.2. Synthesis of Nitrogen-Doped Hydrothermally Reduced Graphene Oxide (N-HtrGO). N-HtrGO was synthesized using a procedure reported in a previous study by our research group.[6] In brief, 15 mL of a GO solution (4 g L^{-1} aqueous solution) was diluted with 15 mL of Millipore Type 1 ultrapure water and sonicated for 30 min. Then, the same mass of urea (60 mg) as GO was added to the solution and mixed for 60 min using an ultrasonic bath. The mixture was transferred to a Teflon-lined stainless steel autoclave. The autoclave was placed in an oven at 150 °C for 12 h to perform a hydrothermal treatment. The resulting hydrogel was separated from the supernatant fluid by centrifugation using water and ethanol. The as-synthesized N-HtrGO was immediately dispersed in ethanol to avoid restacking of the reduced graphene oxide sheets.

2.3. N-HtrGO/PQ Preparation. N-HtrGO/PQ was prepared by using a simple physical absorption method. N-HtrGO dispersed in ethanol (0.5 mg mL^{-1}) was mixed with different amounts of PQ via sonication for 60 min to make N-HtrGO/*X*PQ (X is the percentage of PQ in the N-HtrGO/PQ by mass). Six different PQ mass percentages (20, 25, 30, 35, 50, and 75%) were produced.

2.4. Material Characterization. The morphologies of N-HtrGO and N-HtrGO/PQ were studied by scanning electron microscopy (SEM) using a JEOL 7000F. Transmission electron microscopy (TEM), scanning transmission electron microscopy (STEM), and electron energy-loss spectroscopy (EELS) mapping were conducted using a Talos 200X microscope. Brunauer–Emmett–Teller (BET) analysis was used to investigate the specific surface area and pore size distribution of the samples. FTIR analysis was conducted to determine the components of the synthesized composite. X-ray photoelectron spectroscopy (XPS) was employed to study the near-surface elemental composition of the composite using a Thermo Fisher Scientific K-Alpha XPS System. CasaXPS was used to fit the data, and the spectra were charge-corrected according to adventitious carbon (B.E. = 284.8 eV).[57] X-ray diffraction (XRD) measurements were performed with Cu Kα radiation at the McMaster Analytical X-ray Diffraction Facility (MAX).

2.5. Electrochemical Evaluation. Electrochemical studies were performed by using a three-electrode electrochemical system and a potentiostat (Biologic, France). An Ag/AgCl (Pine Research) reference electrode was used along with a graphite rod as a counter electrode in all experiments. A glassy carbon electrode (Pine Research) with a geometric area of 0.196 cm^2 was used as a working electrode. To prepare the ink, 60 μL of a Nafion-containing solution (5% in a mixture of lower aliphatic alcohols and water) was mixed with 2 mL of an ethanol solution containing 0.5 mg mL^{-1} of N-HtrGO/PQ. Electrodes were prepared by drop-casting the ink on the glassy carbon electrodes. Four different active material loadings were tested: 25, 50, 75, and 100 μg cm^{-2}. The electrodes were subjected to 50 preconditioning cycles of CV at 100 mV s^{-1} prior to the start of the evaluation. The electrochemical capacitance of the synthesized material was evaluated using CV and galvanostatic charge/discharge (GCD). CVs were performed at 5, 10, 50, 100, 200, 300, 400, and 500 mV s^{-1} scan rates. All experiments were carried out in 1 M H_2SO_4 as an acidic aqueous electrolyte. Nitrogen gas was purged continuously into the electrolyte during the experiments. Electrochemical impedance spectroscopy (EIS) measurements were conducted in a frequency range of 100 Hz to 1 MHz using the amplitude of the sinusoidal voltage. GCD was performed at three current densities (1, 5, and 10 A g^{-1}).

The specific capacitance was calculated by cyclic voltammetry (C_{cv}) using eq 1:

$$C_{cv} = \frac{\int I \, d\nu}{2\nu \Delta V m} \tag{1}$$

where I is the current, m is the mass of active materials, ΔV is the working potential window, and ν is the scan rate.[58]

The specific capacitance from galvanostatic charge/discharge (C_{GCD}) experiments was calculated using eq 2:

$$C_{GCD} = \frac{I}{(dV/dt)m} \tag{2}$$

where I is the current, m is the mass of active material, and dV/dt is the slope of the discharge curve.[58]

3. RESULTS AND DISCUSSION

N-HtrGO/PQ composite materials were prepared with varying component ratios, and the composite containing 30 wt % PQ (denoted N-HtrGO/30PQ) was found to provide the highest capacitance and was therefore the composition most extensively characterized. The morphologies of N-HtrGO and N-HtrGO/30PQ were investigated using SEM and TEM. Figure 1a–d shows TEM images of N-HtrGO and N-HtrGO/PQ. Both N-HtrGO and N-HtrGO/PQ showed wrinkled 2D sheet-like structures. The folded and crumpled morphology of these materials has been speculated to play a role in reducing the restacking of graphene sheets and providing interlayer spacing, which improves the electrochemical performance.[2] EELS was used to investigate the elemental distribution of light elements, including carbon, oxygen, and nitrogen, in the

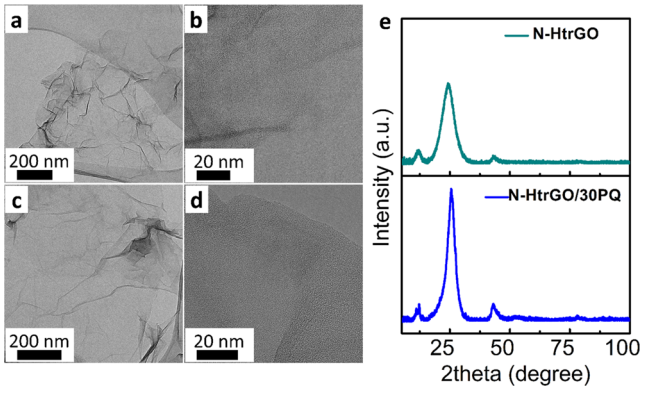

Figure 1. TEM images of (a, b) N-HtrGO and (c, d) N-HtrGO/30PQ. (e) XRD patterns of N-HtrGO (green) and N-HtrGO/30PQ (blue).

https://doi.org/10.1021/acsomega.3c04836
ACS Omega 2024, 9, 10080–10089

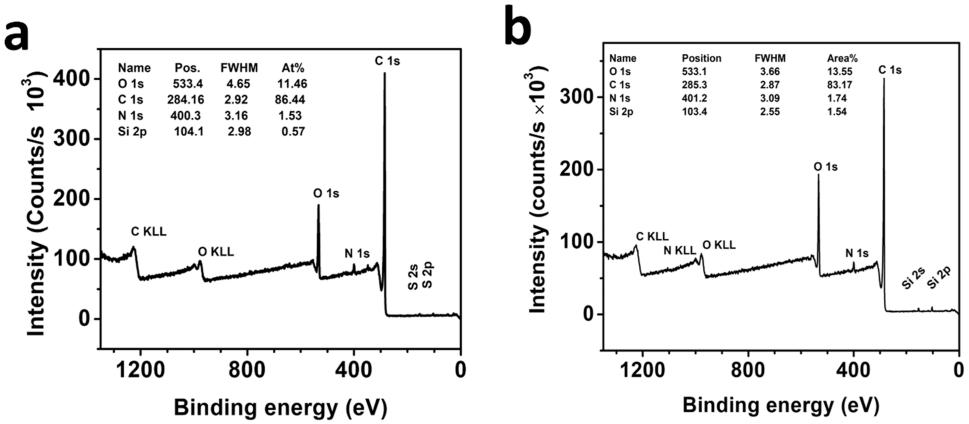

Figure 2. XPS survey spectra for (a) N-HtrGO and (b) N-HtrGO/30PQ.

samples. The results are presented in Figure S1, which indicates that nitrogen was homogeneously dispersed throughout the reduced graphene oxide structures. SEM images are displayed in Figure S2a,b. Reduced graphene oxide layers can be observed in both figures.

The crystallinity of the samples was studied by using X-ray diffraction (Figure 1e). The XRD patterns of N-HtrGO showed two peaks at $2\theta = 23$ and 43°, which were attributed to the (002) and (101) lattice planes of the graphitic structure of N-HtrGO. The XRD peak at $2\theta = 12°$ was related to the (001) crystal plane of graphene oxide and was indicative of the presence of functional groups like hydroxyl and epoxy that are characteristic of graphene oxide. The peak at $2\theta = 78°$ corresponded to the (002) crystal plane of graphite, indicating a high degree of graphitization and crystallinity in the material. The XRD pattern of N-HtrGO/PQ showed characteristic peaks of graphite, indicating that the graphitic structure of the N-HtrGO has not changed after adding the organic molecules.

X-ray photoelectron spectroscopy was used to study the bonding configurations and the near-surface elemental composition of the prepared materials. The XPS survey spectra of N-HtrGO and N-HtrGO/PQ are presented in Figure 2a,b and were used to calculate the near-surface elemental composition of the materials, as shown in Table 1. In

Table 1. Chemical Composition of N-HtrGO and N-HtrGO/30PQ

sample	C (atom %)	O (atom %)	N (atom %)
N-HtrGO	86.9	11.5	1.6
N-HtrGO/PQ	84.5	13.8	1.7

both samples, the presence of nitrogen with similar compositions was observed, verifying successful nitrogen doping and indicating that compositing with PQ does not dramatically impact doping levels of N-HtrGO. The high-resolution N 1s, C 1s, and O 1s spectra of both samples were deconvoluted into their contributing components (Figures S3 and S4). The N 1s spectra (Figure S3a,b) showed a combination of pyridinic-N (ca. 398.05 eV), pyrrolic-N (ca. 399.45 eV), and quaternary (ca. 401.85 eV) nitrogen. Deconvolution of the high-resolution C 1s spectra for N-HtrGO (Figure S4a,b) provides six distinct components corresponding to the graphitic carbon framework for sp^2-hybridized graphitic carbon, C═C (284.30 eV), $\pi-\pi$ (290.71 eV), C−C, C−H (284.8 eV), carbonyls (C═O; 287.60 eV), carboxylic acids (O−C═O; 288.80 eV), C−N (285.80 eV), and C−O in epoxy and hydroxyl (C−OH/C−O−C; 286.50 eV). Deconvolution of the high-resolution C 1s spectra for N-HtrGO/PQ (Figure S3d) shows the same five peaks. The Pi−Pi* peak in sample 2 could be attributed to $\pi-\pi$ interactions between PQ and N-HtrGO.[59,60] The high-resolution O 1s spectra of the samples are presented in Figure S4c,d. The peak at 531.18 eV could be attributed to C═O of 9,10-phenanthrenequinone.[60−62]

FTIR spectroscopy was used to study the functional groups on N-HtrGO/PQ and the interactions between N-HtrGO and PQ. FTIR spectra of PQ and N-HtrGO/PQ are displayed in Figure 3 and the spectra of N-HtrGO in Figure S5. In the

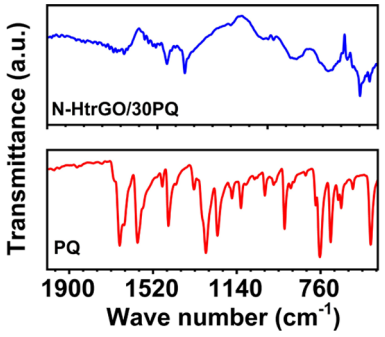

Figure 3. FTIR spectra of N-HtrGO/30PQ (blue, top) and PQ (red, bottom).

spectra of pure PQ, the characteristic peaks of PQ molecules are shown at 706, 1283, 1594, and 1676 cm^{-1}. For the N-HtrGO/PQ composite, the absorption peaks are observed at 1670 cm^{-1}, which is attributed to stretching vibrations of the C═O bonds, and 1589 cm^{-1}, which corresponds to the aromatic C═C bonds. Also, the peaks are observed at 1280 cm^{-1}, corresponding to the stretching vibrations of the C−O bonds in the aromatic ring, and at 770 cm^{-1}, which is attributed to out-of-plane C−H deformation vibrations. The PQ molecule characteristic peaks can be observed in the N-HtrGO/PQ spectra, confirming the presence of PQ in the N-HtrGO/PQ composite. For the N-HtrGO/PQ spectra, C−H out-of-plane deformation vibrations exhibit a blue shift, while the C═O peak and the C−O peak (which indicates aromatic skeleton stretching vibrations) display a red shift, which postulates the strong $\pi-\pi$ interaction between the PQ molecules and N-HtrGO sheets.[63]

https://doi.org/10.1021/acsomega.3c04836
ACS Omega 2024, 9, 10080−10089

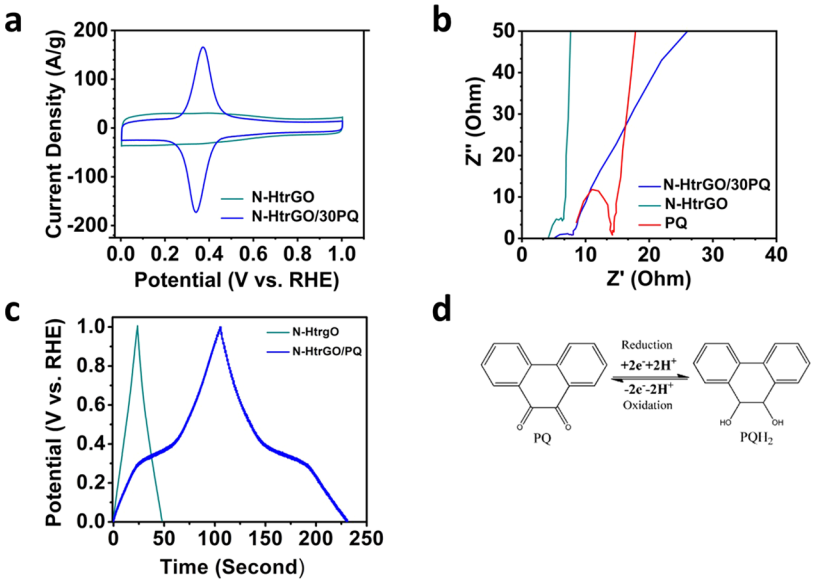

Figure 4. (a, b) Nyquist plot of PQ (red), N-HtrGO (green), and N-HtrGO/30PQ (blue), (c) GCD curves of N-HtrGO and N-HtrGO/30PQ at 5 A g^{-1} in 1 M sulfuric acid, and (d) schematic of PQ reversible redox reaction.

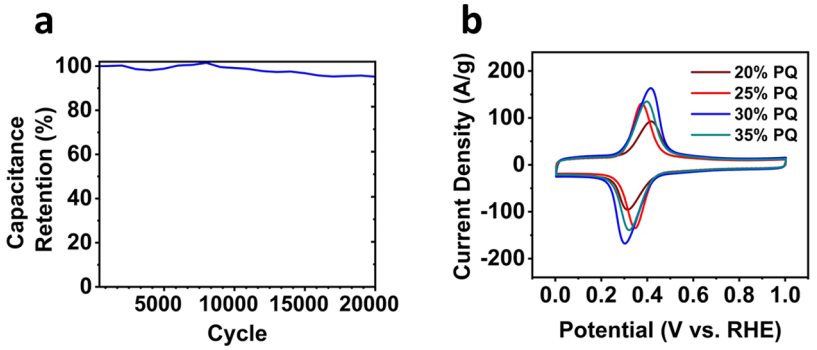

Figure 5. (a) CV curves of N-HtrGO/30PQ with different PQ% in the composites at 50 mV s^{-1} in 1 M sulfuric acid and (b) cycling stability of N-HtrGO/30PQ at a scan rate of 100 mV s^{-1} in 1 M sulfuric acid.

The nitrogen adsorption/desorption isotherms of N-HtrGO and N-HtrGO/30PQ are presented in Figure S6. The average pore diameter was 3.8 nm for the N-HtrGO sample (Figure S6a), and the specific surface area of N-HtrGO was calculated to be 374.5 m^2 g^{-1} using BET. The rising trend observed in the relative pressure below 0.2 shows the presence of micropores in the sample. The hysteresis loop in the relative pressure P/P_0 ranging from 0.2 to 0.9 is attributed to mesopores that existed in the sample. The sharp increase in N_2 adsorption at relative pressures higher than 0.9 suggests the presence of macropores in the samples. The nitrogen adsorption/desorption isotherm of N-HtrGO/30PQ is displayed in Figure S6b. A similar hysteresis loop was observed in the relative pressure P/P_0 ranging from 0.2 to 0.9, indicating the presence of mesopores. The specific surface area decreased significantly after adding PQ to the N-HtrGO from 374.5 to 93.43 m^2 g^{-1}, which could be due to the adsorption of PQ molecules on the surface of N-HtrGO that covers a portion of pores existing in the structure. This trend has been reported before in the literature.[63]

The electrochemical performance of the synthesized composite was evaluated by cyclic voltammetry from 0 to 1.0 V vs the reversible hydrogen electrode (RHE) at different scan rates (5, 50, and 100 mV s^{-1}) in 1 M H_2SO_4 electrolyte. The CV curves of N-HtrGO and N-HtrGO/PQ are presented in Figure 4a. The CV profile of N-HtrGO shows mostly electrical double-layer behavior of the carbon materials with a small pseudocapacitance contribution, which can be attributed to the presence of redox-active pyrrolic and pyridinic nitrogen in the N-HtrGO structure, or the oxygen species observed by XPS that might be capable of providing redox activity (i.e., quinone functional groups).[54,55,64] In comparison, a pair of reversible redox peaks can be observed in the N-HtrGO/PQ CV profile at ~0.4 V vs RHE, attributed to the reversible oxidation and reduction of 9,10-phenanthrenequinone. These features demonstrate pseudocapacitance due to the PQ redox reaction in addition to the electrical double-layer capacitance of the underlying N-HtrGO materials. The specific capacitances of N-HtrGO and N-HtrGO/30PQ at 50 mV s^{-1} were calculated to be 257 and 605 F g^{-1}, respectively, indicating that anchoring N-HtrGO with PQ as a redox-active molecule has successfully improved the performance by providing pseudocapacitance. To find the material proportions that yielded the best supercapacitor performance, the N-HtrGO/PQ ratio was optimized by mixing different weight percentages (25, 50, and 75%) of PQ to N-HtrGO in ethanol. Samples were named N-HtrGO/XPQ, where X is the percentage of PQ in the sample. CV was used to evaluate the performance of prepared samples, and these results are presented in Figure S7. The sample with

https://doi.org/10.1021/acsomega.3c04836
ACS Omega 2024, 9, 10080−10089

25% PQ showed a higher capacitance and thus a better performance than that with 50% PQ and 75% PQ. Furthermore, new samples with PQ percentages close to 25% were prepared with 20, 30, and 35% PQ. The results indicated that by increasing the percentage of PQ from 20 to 30%, the capacitance increased from 495 to 605 F g^{-1}. Then, the performance slightly decreased when the PQ percentage was increased from 30 to 35% (Figure 5a). Increasing the added amount of PQ to 30% could possibly allow for the formation of a $\pi-\pi$ network between the N-HtrGO substrate and phenanthrenequinone molecules. The presence of the $\pi-\pi$ network could increase the delocalization of electrons in the material and consequently increase the overall electrical conductivity and performance of the electrode.[49] The performance deteriorated by increasing the PQ percentage to values higher than 30%, which could be due to the adsorption of PQ molecules onto each other and forming an $\pi-\pi$ network between PQ molecules as a result of the presence of excess PQ. This type of $\pi-\pi$ network is associated with PQ aggregation[65] and can hinder charge transfer from the electrolyte to the electrode. Thus, the electrode with 30% PQ, N-HtrGO/30PQ was identified as the optimum electrode for further investigations, as it contained enough PQ to maximize capacity without formation of PQ aggregates.

The specific capacitance of the N-HtrGO/30PQ electrode was calculated at different scan rates (Figure S8). By increasing the scan rate from 50 to 400, 84.6% of the initial capacitance was achieved. The high-rate capability of this electrode could be due to the fast protonation/deprotonation of the carbonyl groups of the 9,10-phenanthrenequinone. There were no distortions observed in the CV curve shapes at different scan rates (Figure S9), indicating the fast response of the electrode as a result of the presence of redox-active organic molecules.[66−68]

The stability of the N-HtrGO/PQ electrode was investigated by applying 20,000 repeated CV cycles from 0 to 1.0 V vs RHE as shown in Figure 5b. After 1000 cycles, no capacitance loss was observed, and in fact, the capacitance even increased slightly, likely owing to gradually increased electrolyte penetration into the electrode. After 20,000 cycles, the overall capacitance retention was 94.9%, which is higher than the stability of N-HtrGO previously reported by our research group.[6] The high stability is likely attributed to strong $\pi-\pi$ interactions that spontaneously develop between N-HtrGO and PQ molecules through facile noncovalent modification.[45]

Galvanostatic charge/discharge was also used to investigate the electrochemical behavior of the samples in 1 M H_2SO_4 from 0 to 1 V vs RHE at three different current densities, 5, 10, and 20 A g^{-1}, in a three-electrode system. The GCD curves of N-HtrGO and N-HtrGO/PQ are presented in Figure 4c. N-HtrGO showed an EDLC triangular profile, while the N-HtrGO/30PQ profile deviated from a perfect triangular shape. The triangular portion of the GCD curve shows the presence of electrical double-layer behavior, while the deviation in a triangular shape in the form of a plateau indicates the existence of pseudocapacitive behavior, in agreement with the results of CV evaluation. The specific capacitance was calculated to be 630 F g^{-1} at 5 A g^{-1} by using GCD. The GCD profiles of N-HtrGO/30PQ at different scan rates are presented in Figure S10. The reversible redox reaction occurring in the PQ molecules is presented in Figure 4d.[69] Furthermore, EIS was carried out at open-circuit potential to study ion transport behavior. The Nyquist plots of PQ, N-HtrGO, and N-HtrGO/30PQ electrodes are presented in Figure 4b, showing a semicircle in the high-frequency region and an inclined line in the low-frequency region. The almost vertical line in the low-frequency region indicates a good ion diffusion process.[70] The equivalent circuits shown in Figure S11 were used to fit the obtained Nyquist plot. The circuit for N-HtrGO/30PQ includes one resistor attributed to the electrolyte solution and two capacitors due to the presence of an electrical double-layer current (C2) and Faradaic current (C3). One other resistor exists due to charge-transfer resistance. This equivalent circuit also includes a Warburg element, corresponding to the deviation from the vertical line in the low-frequency region, indicating that the Warburg length is slightly higher.[70] The circuit for N-HtrGO includes only one capacitor (C2) attributed to electrical double-layer capacitance, as this sample did not show appreciable redox (Faradaic) processes associated with the inclusion of PQ in the N-HtrGO/30PQ sample. The vertical line in the low-frequency region of the Nyquist plot corresponds to the fast ion diffusion in N-HtrGO, indicating the capacitive behavior.[70] The charge-transfer resistances were calculated to be 3.92, 2.80, and 3.27 Ω for pure PQ, N-HtrGO, and N-HtrGO/30PQ, respectively. The low charge-transfer resistance in the N-HtrGO/PQ electrode can potentially be attributed to $\pi-\pi$ interactions between N-HtrGO and PQ that can increase the electrode conductivity.[49]

The relationship between peak current density and scan rate shows whether ion transfer in the porous electrode structure is diffusion-controlled or surface-controlled. This relationship can be modeled with eq 3:

$$I_p = av^b \tag{3}$$

where I_p is the peak current, ν is the scan rate, and a and b are adjustable parameters. Using eq 3 and the slope of $\log(i)$ vs $\log(\upsilon)$, b can be derived. If b = 1, the process is surface-controlled, and the current is due to EDL formation or surface-confined redox processes. If b = 0.5, the charge storage mechanism is a semi-infinite diffusion-controlled process. This means the current is controlled by the diffusion rate of ions storing charge through EDLC or redox processes. If b falls between 0.5 and 1, the process is a combination of diffusion and capacitive mechanisms.[5] The kinetics of the process in the electrode/electrolyte interface was studied by obtaining the relationship between peak current density and different scan rates (5, 10, 50, 100, 200, 300, 400, and 500 mV s^{-1}) with the CV curves shown in Figure S11a,b. For the N-HtrGO electrode, b is approximately equal to 1, so the redox reaction is adsorption- or surface-controlled. But the N-HtrGO electrode lacks surface redox-active functional groups. The electrode electrochemical reactions are surface-controlled. Therefore, the measured current is due to the electrical double-layer capacitance. The value of b = 0.84 for the N-HtrGO/PQ electrode shows that its operation is dependent on a combination of surface-controlled and diffusion-controlled processes. By adding PQ molecules to the electrode composition, fast surface protonation/deprotonation of PQ molecules occur on the surface and the electrochemical reactions on the N-HtrGO/30PQ electrode are more controlled by the diffusion rate. But the N-HtrGO electrode lacks surface redox-active functional groups. Therefore, the electrode electrochemical reactions are surface-controlled. Furthermore, the contribution of each mechanism was calculated using Dunn's analysis.[71,72] The results are presented in Figure 6. Figure 6a,b shows CV curves of N-HtrGO and N-

https://doi.org/10.1021/acsomega.3c04836
ACS Omega 2024, 9, 10080−10089

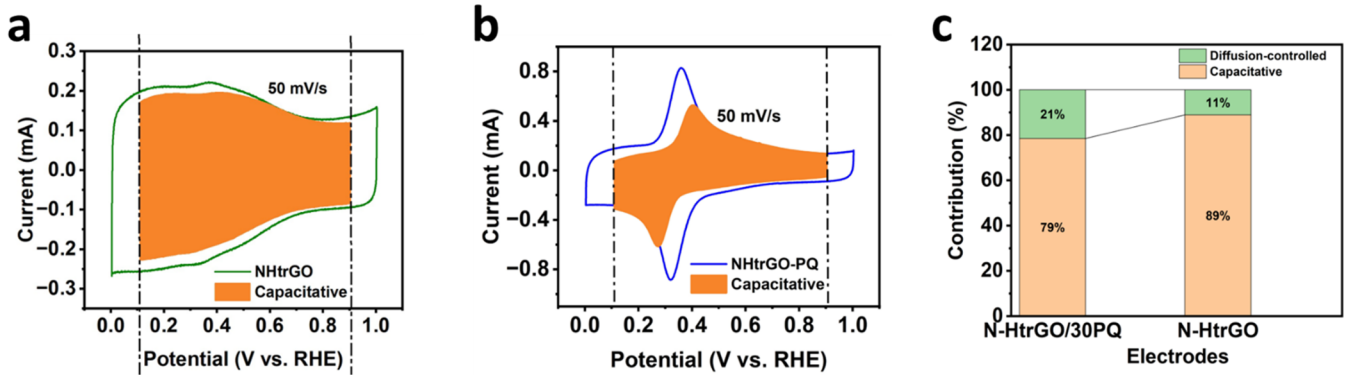

Figure 6. CV curves of (a) N-HtrGO, (b) N-HtrGO/30PQ at 50 mV/s, and (c) bar chart indicating the contribution of different reaction mechanisms.

HtrGO/30PQ with the orange area indicating the capacitive contribution in each electrode. Figure 6c shows that after adding PQ molecules to the electrode composition, the reaction is more controlled by the diffusion rate since the surface redox reactions are fast.

4. CONCLUSIONS

In this study, a composite was developed through a simple physical adsorption of 9,10-phenanthrenequinone on nitrogen-doped reduced graphene oxide (N-HtrGO/PQ) and applied as a supercapacitor material which benefited from the synergistic behavior of the combined materials. In 1 M H_2SO_4, N-HtrGO/PQ with an optimized composition of 30 wt % PQ achieved a specific capacitance of 605 F g^{-1} measured by CV at a scan rate of 50 mV s^{-1}. The CV profile of the composite revealed a combination of electrical double-layer capacitance and pseudocapacitance. The electrical double-layer capacitance resulted from the N-HtrGO with a high surface area (374.5 m^2 g^{-1}) and high electrical conductivity as confirmed by EIS, while 9,10-phenanthrenequinone provided the composite with pseudocapacitance. The high overall specific capacitance of the composite confirmed the capability of PQ molecules to improve the low energy density of EDLC materials via a simple adsorption modification. This modification furthermore provided a 94.9% capacitance retention after 20,000 CV cycles, likely resulting from strong $\pi-\pi$ interactions between the N-HtrGO sheets and PQ molecules as indicated by FTIR analysis. These findings indicate that compositing redox-active organic molecules with nitrogen-doped reduced graphene oxide via noncovalent interactions can provide a simple and effective technique to develop electrode materials for supercapacitor applications. Furthermore, now that we have a suitable material that has been tested in a three-electrode setup, the next steps will be to integrate into a two-electrode device that will include the important steps of electrode preparation optimization, component selection, and device engineering. Particularly, this electrode could be suitable for application in asymmetric supercapacitors due to having higher energy density.

■ ASSOCIATED CONTENT

Supporting Information

The Supporting Information is available free of charge at https://pubs.acs.org/doi/10.1021/acsomega.3c04836.

STEM images of N-HtrGO and N-HtrGO/30PQ; SEM images of N-HtrGO and N-HtrGO/30PQ; high-resolution XPS spectra; nitrogen adsorption/desorption isotherms of N-HtrGO and N-HtrGO/30PQ; cyclic voltammograms of samples; galvanostatic charge/discharge curves; equivalent circuit of samples. (PDF)

■ AUTHOR INFORMATION

Corresponding Author

Drew Higgins − *Department of Chemical Engineering, McMaster University, Hamilton, Ontario L8S 4L7, Canada;* orcid.org/0000-0002-0585-2670; Email: higgid2@mcmaster.ca

Authors

Navid Noor − *Department of Chemical Engineering, McMaster University, Hamilton, Ontario L8S 4L7, Canada*

Thomas Baker − *Department of Chemical Engineering, McMaster University, Hamilton, Ontario L8S 4L7, Canada*

Hyejin Lee − *Department of Chemical Engineering, McMaster University, Hamilton, Ontario L8S 4L7, Canada; School of Chemical and Biological Engineering, Institute of Chemical Process (ICP), and Institute of Engineering Research, Seoul National University, Seoul 08826, Republic of Korea*

Elliot Evans − *Department of Chemical Engineering, McMaster University, Hamilton, Ontario L8S 4L7, Canada*

Shayan Angizi − *Department of Chemical Engineering, McMaster University, Hamilton, Ontario L8S 4L7, Canada;* orcid.org/0000-0002-5345-4271

Jeffrey Daniel Henderson − *Surface Science Western, Western University, London, Ontario N6G 0J3, Canada*

Amirhossein Rakhsha − *Department of Chemical Engineering, McMaster University, Hamilton, Ontario L8S 4L7, Canada*

Complete contact information is available at: https://pubs.acs.org/10.1021/acsomega.3c04836

Notes

The authors declare no competing financial interest.

■ ACKNOWLEDGMENTS

This work was funded by the Natural Sciences and Engineering Research Council of Canada (NSERC) Alliance Program, Nissan North America Inc., and McMaster University's Faculty of Engineering. Electron microscopy was performed at the Canadian Centre for Electron Microscopy (CCEM) at McMaster University. X-ray photoelectron spectroscopy was performed at the Open Center for the Characterization of Advanced Materials (OCCAM) at the University of Toronto.

XPS analysis was performed at the Surface Science Western at Western University.

REFERENCES

(1) Lee, H.-J.; Noor, N.; Gumeci, C.; Dale, N.; Parrondo, J.; Higgins, D. C. Understanding the Impact of the Morphology, Phase Structure, and Mass Fraction of MnO 2 within MnO 2/Reduced Graphene Oxide Composites for Supercapacitor Applications. *J. Phys. Chem. C* **2022**, *126*, 13004−13014.

(2) Shao, Y.; El-Kady, M. F.; Sun, J.; Li, Y.; Zhang, Q.; Zhu, M.; Wang, H.; Dunn, B.; Kaner, R. B. Design and Mechanisms of Asymmetric Supercapacitors. *Chem. Rev.* **2018**, *118* (18), 9233−9280.

(3) Liu, W.; Zhang, M.; Li, M.; Li, B.; Zhang, W.; Li, G.; Xiao, M.; Zhu, J.; Yu, A.; Chen, Z. Advanced Electrode Materials Comprising of Structure-Engineered Quantum Dots for High-Performance Asymmetric Micro-Supercapacitors. *Adv. Energy Mater.* **2020**, *10* (8), No. 1903724.

(4) Bazan-Aguilar, A.; Ponce-Vargas, M.; Caycho, C. L.; La Rosa-Toro, A.; Baena-Moncada, A. M. Highly Porous Reduced Graphene Oxide-Coated Carbonized Cotton Fibers as Supercapacitor Electrodes. *ACS Omega* **2020**, *5* (50), 32149−32159.

(5) Fleischmann, S.; Mitchell, J. B.; Wang, R.; Zhan, C.; Jiang, D. E.; Presser, V.; Augustyn, V. Pseudocapacitance: From Fundamental Understanding to High Power Energy Storage Materials. *Chem. Rev.* **2020**, *120* (14), 6738−6782.

(6) Lee, H.-J.; Abdellah, A.; Ismail, F. M.; Gumeci, C.; Dale, N.; Parrondo, J.; Higgins, D. C. Understanding the impact of nitrogen doping and/or amine functionalization of reduced graphene oxide via hydrothermal routes for supercapacitor applications. *Electrochim. Acta* **2021**, *397*, No. 139241.

(7) Horn, M.; Gupta, B.; MacLeod, J.; Liu, J.; Motta, N. Graphene-based supercapacitor electrodes: Addressing challenges in mechanisms and materials. *Curr. Opin. Green Sustainable Chem.* **2019**, *17*, 42−48.

(8) El-Kady, M. F.; Strong, V.; Dubin, S.; Kaner, R. B. Laser Scribing of High-Performance and Flexible Graphene-Based Electrochemical Capacitors. *Science* **2012**, *335* (6074), 1326−1330.

(9) Liu, W.; Li, M.; Jiang, G.; Li, G.; Zhu, J.; Xiao, M.; Zhu, Y.; Gao, R.; Yu, A.; Feng, M.; Chen, Z. Graphene Quantum Dots-Based Advanced Electrode Materials: Design, Synthesis and Their Applications in Electrochemical Energy Storage and Electrocatalysis. *Adv. Energy Mater.* **2020**, *10* (29), No. 2001275.

(10) Noor, N.; Pajootan, E.; Mirzaei, P.; Bahrami, S. H. A highly selective carbon paste electrode enhanced by Cu-encapsulated poly (amidoamine) for the simultaneous detection of organic and inorganic contaminants. *Can. J. Chem. Eng.* **2023**, *101*, 5759−5771.

(11) Kang, S. H.; Lee, G. Y.; Lim, J.; Kim, S. O. CNT−rGO Hydrogel-Integrated Fabric Composite Synthesized via an Interfacial Gelation Process for Wearable Supercapacitor Electrodes. *ACS Omega* **2021**, *6* (30), 19578−19585.

(12) Chabot, V.; Higgins, D.; Yu, A.; Xiao, X.; Chen, Z.; Zhang, J. A review of graphene and graphene oxide sponge: material synthesis and applications to energy and the environment. *Energy Environ. Sci.* **2014**, *7* (5), 1564−1596.

(13) Akerdi, A. G.; Es'haghzade, Z.; Bahrami, S.; Arami, M. Comparative Study of GO and Reduced GO Coated Graphite Electrodes for Decolorization of Acidic and Basic Dyes from Aqueous Solutions through Heterogeneous Electro-Fenton Process. *J. Environ. Chem. Eng.* **2017**, *5*, 2313−2324.

(14) Akerdi, A. G.; Bahrami, S. H.; Arami, M.; Noormohammadi, N. Discoloration of Cationic Dye by Using Reduced Graphene Oxide Modified Carbon Electrode and Magnetite Nanoparticles Within Heterogeneous Electro-fenton Process. *J. Color Sci. Technol.* **2021**, *15* (1), 1−11.

(15) Noor, N.; Pajootan, E.; Mirzaei, P.; Bahrami, S. H.; Daryani, A. S. A Highly Selective Carbon Paste Electrode Enhanced by Cu-Encapsulated Pamam for the Simultaneous Detection of Organic and Inorganic Contaminants. *Can. J. Chem. Eng.* **2023**, *101*, 5759−5771.

(16) Makkar, P.; Ghosh, N. N. Facile Synthesis of MnFe2O4 Hollow Sphere-Reduced Graphene Oxide Nanocomposites as Electrode Materials for All-Solid-State Flexible High-Performance Asymmetric Supercapacitors. *ACS Appl. Energy Mater.* **2020**, *3* (3), 2653−2664.

(17) Zhang, L. L.; Zhou, R.; Zhao, X. Graphene-based materials as supercapacitor electrodes. *J. Mater. Chem.* **2010**, *20* (29), 5983−5992.

(18) Wang, X.; Sun, G.; Routh, P.; Kim, D.-H.; Huang, W.; Chen, P. Heteroatom-doped graphene materials: syntheses, properties and applications. *Chem. Soc. Rev.* **2014**, *43* (20), 7067−7098.

(19) Shi, H. H.; Jang, S.; Reza-Ugalde, A.; Naguib, H. E. Hierarchically Structured Nitrogen-Doped Multilayer Reduced Graphene Oxide for Flexible Intercalated Supercapacitor Electrodes. *ACS Appl. Energy Mater.* **2020**, *3* (1), 987−997.

(20) Moustafa, E.; El Nady, J.; Kashyout, A. E.-H. B.; Shoueir, K.; El-Kemary, M. Fabrication of High Yield Photoluminescent Quantized Graphene Nanodiscs for Supercapacitor Devices. *ACS Omega* **2021**, *6* (36), 23090−23099.

(21) Alipour, S.; Mousavi-Khoshdel, S. M. Investigation of the electrochemical behavior of functionalized graphene by nitrophenyl groups as a potential electrode for supercapacitors. *Electrochim. Acta* **2019**, *317*, 301−311.

(22) Jiao, L.; Hu, Z.; Ma, F.; He, Y.; Zhou, Q.; Xiao, L.; Lv, L.; Yang, Y. A novel organic molecule electrode based on organic polymer functionalized graphene for supercapacitor with high-performance. *J. Energy Storage* **2022**, *52*, No. 104777.

(23) Najafi, M. D.; Kowsari, E.; Naderi, H. R.; Tafreshi, S. S.; Chinnappan, A.; Ramakrishna, S.; de Leeuw, N. H.; Ehsani, A. High-performance symmetric supercapacitor based on new functionalized graphene oxide composites with pyrimidine nucleotide and nucleoside. *J. Mol. Liq.* **2022**, *348*, No. 118381.

(24) Zhang, L.; Qing, X.; Chen, Z.; Wang, J.; Yang, G.; Qian, Y.; Liu, D.; Chen, C.; Wang, L.; Lei, W. All Pseudocapacitive Nitrogen-Doped Reduced Graphene Oxide and Polyaniline Nanowire Network for High-Performance Flexible On-Chip Energy Storage. *ACS Appl. Energy Mater.* **2020**, *3* (7), 6845−6852.

(25) Huang, M.; Li, F.; Zhao, X. L.; Luo, D.; You, X. Q.; Zhang, Y. X.; Li, G. Hierarchical ZnO@MnO2 core-shell pillar arrays on ni foam for binder-free supercapacitor electrodes. *Electrochim. Acta* **2015**, *152*, 172−177.

(26) Senthilkumar, N.; Venkatachalam, V.; Kandiban, M.; Vigneshwaran, P.; Jayavel, R.; Vetha Potheher, I. Studies on electrochemical properties of hetarolite (ZnMn2O4) nanostructure for supercapacitor application. *Physica E* **2019**, *106*, 121−126.

(27) Isacfranklin, M.; Yuvakkumar, R.; Ravi, G.; Saravanakumar, B.; Pannipara, M.; Al-Sehemi, A. G.; Velauthapillai, D. Quaternary Cu2FeSnS4/PVP/rGO Composite for Supercapacitor Applications. *ACS Omega* **2021**, *6* (14), 9471−9481.

(28) Kathalingam, A.; Ramesh, S.; Yadav, H. M.; Choi, J. H.; Kim, H. S.; Kim, H. S. Nanosheet-like ZnCo2O4@nitrogen doped graphene oxide/polyaniline composite for supercapacitor application: Effect of polyaniline incorporation. *J. Alloys Compd.* **2020**, *830*, 154734.

(29) Qu, K.; You, Y.; Qi, H.; Shi, C.; Sun, Z.; Huang, Z.; Yuan, B.; Guo, Z. Fungus Bran-Derived Porous N-Doped Carbon-Zinc Manganese Oxide Nanocomposite Positive Electrodes toward High-Performance Asymmetric Supercapacitors. *J. Phys. Chem. C* **2020**, *124* (29), 15713−15722.

(30) Li, M.; Liu, J.; Zhang, T.; Song, X.; Chen, W.; Chen, L. 2D redox-active covalent organic frameworks for supercapacitors: Design, synthesis, and challenges. *Small* **2021**, *17* (22), No. 2005073.

(31) Venkateshalu, S.; Grace, A. N. MXenes—A new class of 2D layered materials: Synthesis, properties, applications as supercapacitor electrode and beyond. *Appl. Mater. Today* **2020**, *18*, No. 100509.

(32) Huang, X.; Huang, J.; Yang, D.; Wu, P. A multi-scale structural engineering strategy for high-performance MXene hydrogel supercapacitor electrode. *Adv. Sci.* **2021**, *8* (18), No. 2101664.

(33) Xiao, L.; Hu, Z.; He, Y.; Jiao, L.; Lv, L.; Yin, Q.; Wei, Q.; Li, Z.; Yang, Y. Aqueous Electrolyte Asymmetric Supercapacitors Based on

https://doi.org/10.1021/acsomega.3c04836
ACS Omega 2024, 9, 10080−10089

the 5-Hydroxyindole Molecule Electrode and MXene with Efficient Energy Storage. *ACS Appl. Energy Mater.* **2023**, *6* (1), 68−78.
(34) Vivas, L.; Jara, A.; Garcia-Garfido, J. M.; Serafini, D.; Singh, D. P. Facile Synthesis and Optimization of CrOOH/rGO-Based Electrode Material for a Highly Efficient Supercapacitor Device. *ACS Omega* **2022**, *7* (46), 42446−42455.
(35) Ega, S. P.; Srinivasan, P. Quinone materials for supercapacitor: Current status, approaches, and future directions. *J. Energy Storage* **2022**, *47*, 103700.
(36) Wang, P.; Wu, Q.; Han, L.; Wang, S.; Fang, S.; Zhang, Z.; Sun, S. Synthesis of conjugated covalent organic frameworks/graphene composite for supercapacitor electrodes. *RSC Adv.* **2015**, *5* (35), 27290−27294.
(37) Ma, Y.; Chen, Y.; Xin, C.; Cheng, Y.; Li, Q.; Xu, H. A High-Performance Redox Electrochemical Capacitor: Confinement of Sodium Anthraquinone-2-Sulfonate in Porous Carbons with Electric-Field Assistance. *ACS Appl. Energy Mater.* **2023**, *6* (12), 6532−6542.
(38) N'Diaye, J.; Bagchi, R.; Howe, J. Y.; Lian, K. Redox Active Organic-Carbon Composites for Capacitive Electrodes: A Review. *Sustainable Chem.* **2021**, *2* (3), 407−440.
(39) Guo, B.; Yang, Y.; Hu, Z.; An, Y.; Zhang, Q.; Yang, X.; Wang, X.; Wu, H. Redox-active organic molecules functionalized nitrogen-doped porous carbon derived from metal-organic framework as electrode materials for supercapacitor. *Electrochim. Acta* **2017**, *223*, 74−84.
(40) Shi, R.; Han, C.; Duan, H.; Xu, L.; Zhou, D.; Li, H.; Li, J.; Kang, F.; Li, B.; Wang, G. Redox-Active Organic Sodium Anthraquinone-2-Sulfonate (AQS) Anchored on Reduced Graphene Oxide for High-Performance Supercapacitors. *Adv. Energy Mater.* **2018**, *8* (31), No. 1802088.
(41) Wedege, K.; Dražević, E.; Konya, D.; Bentien, A. Organic redox species in aqueous flow batteries: redox potentials, chemical stability and solubility. *Sci. Rep.* **2016**, *6* (1), No. 39101.
(42) Dong, Y.; Wang, Y.; Zhang, X.; Lai, Q.; Yang, Y. Carbon-based elastic foams supported redox-active covalent organic frameworks for flexible supercapacitors. *Chem. Eng. J.* **2022**, *449*, No. 137858.
(43) Kuo, T.-R.; Lin, L.-Y.; Kubendhiran, S.; Li, Y.-C.; Chung, R.-J.; Yougbaré, S. Novel incorporation of redox active organic molecule with activated carbon as efficient active material of supercapacitors. *J. Energy Storage* **2022**, *53*, No. 105085.
(44) Liu, J.; Yuan, Y.; Fang, H.; Xu, Y.; Sun, W.; Chen, S.; Wang, Y.; Lv, L.-P. Redox-Active Tetramino-Benzoquinone $\pi-\pi$ Stacking and H-Bonding onto Multiwalled Carbon Nanotubes toward a High-Performance Asymmetric Supercapacitor. *ACS Appl. Energy Mater.* **2022**, *5* (7), 8112−8122.
(45) Ma, F.; Hu, Z.; Jiao, L.; Wang, X.; He, Y.; Yang, Y.; Li, Z. Organic Molecule-Functionalized Reduced Graphene Oxide for All-Carbon Asymmetric Supercapacitor Applications. *ACS Appl. Energy Mater.* **2021**, *4* (6), 5493−5503.
(46) Hou, L.; Kong, C.; Hu, Z.; Wu, B.; Han, Y. Application of multi-active center organic quinone molecular functionalized graphene in fully pseudocapacitive asymmetric supercapacitors. *Nanotechnology* **2021**, *32* (26), No. 265704.
(47) Le Comte, A.; Brousse, T.; Bélanger, D. Simpler and greener grafting method for improving the stability of anthraquinone-modified carbon electrode in alkaline media. *Electrochim. Acta* **2014**, *137*, 447−453.
(48) Xu, L.; Shi, R.; Li, H.; Han, C.; Wu, M.; Wong, C.-P.; Kang, F.; Li, B. Pseudocapacitive anthraquinone modified with reduced graphene oxide for flexible symmetric all-solid-state supercapacitors. *Carbon* **2018**, *127*, 459−468.
(49) Xu, L.; Zhang, Y.; Zhou, W.; Jiang, F.; Zhang, H.; Jiang, Q.; Jia, Y.; Wang, R.; Liang, A.; Xu, J.; Duan, X. Fused heterocyclic molecule-functionalized N-doped reduced graphene oxide by non-covalent bonds for high-performance supercapacitors. *ACS Appl. Mater. Interfaces* **2020**, *12* (40), 45202−45213.
(50) Chen, X.; Wang, H.; Yi, H.; Wang, X.; Yan, X.; Guo, Z. Anthraquinone on porous carbon nanotubes with improved supercapacitor performance. *J. Phys. Chem. C* **2014**, *118* (16), 8262−8270.
(51) Son, E. J.; Kim, J. H.; Kim, K.; Park, C. B. Quinone and its derivatives for energy harvesting and storage materials. *J. Mater. Chem. A* **2016**, *4* (29), 11179−11202.
(52) Youn, H. C.; Bak, S. M.; Kim, M. S.; Jaye, C.; Fischer, D. A.; Lee, C. W.; Yang, X. Q.; Roh, K. C.; Kim, K. B. High-Surface-Area Nitrogen-Doped Reduced Graphene Oxide for Electric Double-Layer Capacitors. *ChemSusChem* **2015**, *8* (11), 1875−1884.
(53) Hong, G.; Han, Y.; Schutzius, T. M.; Wang, Y.; Pan, Y.; Hu, M.; Jie, J.; Sharma, C. S.; Müller, U.; Poulikakos, D. On the Mechanism of Hydrophilicity of Graphene. *Nano Lett.* **2016**, *16* (7), 4447−4453.
(54) Gao, Z.; Zhang, L.; Chang, J.; Wang, Z.; Wu, D.; Xu, F.; Guo, Y.; Jiang, K. Catalytic electrode-redox electrolyte supercapacitor system with enhanced capacitive performance. *Chem. Eng. J.* **2018**, *335*, 590−599.
(55) Gao, Z.; Liu, X.; Chang, J.; Wu, D.; Xu, F.; Zhang, L.; Du, W.; Jiang, K. Graphene incorporated, N doped activated carbon as catalytic electrode in redox active electrolyte mediated supercapacitor. *J. Power Sources* **2017**, *337*, 25−35.
(56) Bharathidasan, P.; Idris, M. B.; Kim, D.-W.; Sivakkumar, S. R.; Devaraj, S. Enhanced capacitance properties of nitrogen doped reduced graphene oxide obtained by simultaneous reduction and nitrogen doping. *FlatChem* **2018**, *11*, 24−31.
(57) Fairley, N.; Fernandez, V.; Richard-Plouet, M.; Guillot-Deudon, C.; Walton, J.; Smith, E.; Flahaut, D.; Greiner, M.; Biesinger, M.; Tougaard, S.; et al. Systematic and collaborative approach to problem solving using X-ray photoelectron spectroscopy. *Appl. Surf. Sci. Adv.* **2021**, *5*, No. 100112.
(58) Nunes, W. G.; Da Silva, L. M.; Vicentini, R.; Freitas, B. G. A.; Costa, L. H.; Pascon, A. M.; Zanin, H. Nickel oxide nanoparticles supported onto oriented multi-walled carbon nanotube as electrodes for electrochemical capacitors. *Electrochim. Acta* **2019**, *298*, 468−483.
(59) Biesinger, M. C. Accessing the robustness of adventitious carbon for charge referencing (correction) purposes in XPS analysis: Insights from a multi-user facility data review. *Appl. Surf. Sci.* **2022**, *597*, No. 153681.
(60) Beamson, G. High Relution XPS of Organic Polymers *Scienta ESCA 300 Database*, ICI plc 1992.
(61) Takahagi, T.; Shimada, I.; Fukuhara, M.; Morita, K.; Ishitani, A. XPS studies on the chemical structure of the stabilized polyacrylonitrile fiber in the carbon fiber production process. *J. Polym. Sci., Part A: Polym. Chem.* **1986**, *24* (11), 3101−3107.
(62) Ohta, T.; Masamichi, Y.; Haruo, K. X-Ray Photoelectron Spectroscopy of p-Benzoquinone, Hydroquinone and Their Halogen-Substituted Derivatives. *Bull. Chem. Soc. Jpn.* **1974**, *47* (5), 1158−1161.
(63) Wang, W.; Yang, Y.; Wang, X.; Zhou, Y.; Zhang, X.; Qiang, L.; Wang, Q.; Hu, Z. Nitrogen-doped hollow carbon spheres functionalized by 9, 10-phenanthrenequinone molecules as a high-performance electrode for asymmetric supercapacitors. *New J. Chem.* **2019**, *43* (16), 6380−6387.
(64) Shi, L.; Liu, S.; He, Z.; Shen, J. Nitrogen-Doped Graphene:Effects of nitrogen species on the properties of the vanadium redox flow battery. *Electrochim. Acta* **2014**, *138*, 93−100.
(65) Anjos, D. M.; Kolesnikov, A. I.; Wu, Z.; Cai, Y.; Neurock, M.; Brown, G. M.; Overbury, S. H. Inelastic neutron scattering, Raman and DFT investigations of the adsorption of phenanthrenequinone on onion-like carbon. *Carbon* **2013**, *52*, 150−157.
(66) Ma, F.; Wang, X.; Hu, Z.; Hou, L.; Yang, Y.; Li, Z.; He, Y.; Zhu, H. Organic Molecular Electrode with Ultrahigh Rate Capability for Supercapacitors. *Energy Fuels* **2020**, *34* (10), 13079−13088.
(67) Wang, H.; Yi, H.; Chen, X.; Wang, X. Asymmetric supercapacitors based on nano-architectured nickel oxide/graphene foam and hierarchical porous nitrogen-doped carbon nanotubes with ultrahigh-rate performance. *J. Mater. Chem. A* **2014**, *2* (9), 3223−3230.

https://doi.org/10.1021/acsomega.3c04836
ACS Omega 2024, 9, 10080−10089

(68) An, N.; Hu, Z.; Wu, H.; Yang, Y.; Lei, Z.; Dong, W. Organic multi-electron redox couple-induced functionalization for enabling ultrahigh rate and cycling performances of supercapacitors. *J. Mater. Chem. A* **2017**, *5* (48), 25420−25430.
(69) Ishioka, T.; Uchida, T.; Teramae, N. Analysis of the redox reaction of 9,10-phenanthrenequinone on a gold electrode surface by cyclic voltammetry and time-resolved Fourier transform surface-enhanced Raman scattering spectroscopy. *Anal. Chim. Acta* **2001**, *449* (1), 253−260.
(70) Hou, L.; Kong, C.; Hu, Z.; Han, Y.; Wu, B. Redox active organic molecule-Emodin modified graphene for high-performance supercapacitors. *J. Electroanal. Chem.* **2021**, *895*, No. 115402.
(71) Wang, J.; Polleux, J.; Lim, J.; Dunn, B. Pseudocapacitive contributions to electrochemical energy storage in TiO2 (anatase) nanoparticles. *J. Phys. Chem. C* **2007**, *111* (40), 14925−14931.
(72) Simon, P.; Gogotsi, Y.; Dunn, B. Where Do Batteries End and Supercapacitors Begin? *Science* **2014**, *343* (6176), 1210−1211.

https://doi.org/10.1021/acsomega.3c04836
ACS Omega 2024, 9, 10080−10089